Korean J. Chem. Eng., 36(12), 2133-2142 (2019)
DOI: 10.1007/s11814-019-0397-5

pISSN: 0256-1115
eISSN: 1975-7220

Poly(phenylene sulfide)-graphite composites for bipolar plates with preferred morphological orientation

Ho-Joon Park*, Jong Seok Woo, and Soo-Young Park*,†**

*Department of Polymer Science & Engineering, Polymeric Nanomaterials Laboratory, School of Applied Chemical Engineering, Kyungpook National University, 80 Daehak-ro, Buk-gu, Daegu 41566, Korea
**Advanced Center of Engineering, Morgan Advanced Materials, 23, Dalseong2cha 4-ro, Guji-myeon, Dalseong-gun, Daegu 43013, Korea
(*Received 25 July 2019 • accepted 26 September 2019*)

Abstract−Bipolar plates in phosphoric acid fuel cells require inertness to phosphoric acid as well as excellent electrical, thermal, and mechanical properties. For this application, we prepared poly(phenylene sulfide) (PPS)-graphite composites with random or ordered graphite orientations by compression and extrusion-compression processes, respectively. Due to current limitations of extruding graphite-filled polymers, only moderately high graphite concentrations were used (up to 40 wt%). The compressed composites contained graphite sheets in a planar orientation (parallel to the pressing direction) and exhibited highly anisotropic electrical and thermal conductivity, with much higher in-plane than through-plane components. In contrast, composites that were extruded prior to compression exhibited randomly oriented graphite due to shearing forces during extrusion and therefore displayed isotropic properties. Thus, their through-plane electrical and thermal conductivity was superior to those of the ordered composite, while the in-plane properties were inferior. Notably, the internal graphitic structure affected the electrical conductivity more than the thermal conductivity. The randomly oriented composite also exhibited superior flexural strength, although the thermal stability of the two composites was almost equal. This study offers insights into the structure-property relationship of PPS-graphite composites as well as the effect of the orientation of conductive two-dimensional fillers on anisotropic properties.

Keywords: Poly(phenylene sulfide), Graphite, Extrusion, Compression, Anisotropy

INTRODUCTION

Owing to their low cost, low weight, and chemical inertness, polymer-graphite composites have been widely researched for use in bipolar plates, which are crucial components in fuel-cell stacks. In particular, for use in phosphoric acid fuel cells, the bipolar plate material must be inert to phosphoric acid as well as have excellent electrical, thermal, and mechanical properties [1-5]. High-performance polymers, such as fluorinated ethylene propylene, poly(vinylidene fluoride), and polyether(ether ketone), are commonly used as the matrix material [6-9]. Poly(phenylene sulfide) (PPS) is one of the best candidates considering the abovementioned requirements, and it can be purchased at low cost [10,11].

One of the most common methods of producing polymer-based composites is compounding using an extruder, as it causes shearing of the composite [22-24]. Shearing improves the dispersion of fillers and produces a random orientation of graphite sheets in polymer-graphite composites. However, when the amount of filler is too high, it exerts high torque in the extruder. Unfortunately, polymer-graphite composites for use in bipolar plates typically comprise more than 80 wt% graphite filler to maximize the electrical, thermal, and chemical properties, which means that the extruder must have high capacity to process these materials. Several attempts have been made to overcome these instrumental difficulties, and it is expected that the production of polymer-graphite-based bipolar plates by compounding will be possible in the near future [25,26]. One of the merits of compounding is that it can be combined with simultaneous injection molding, which eliminates the need for additional patterning of channels—another challenge in the preparation of bipolar plates.

As compounding is not currently possible for the processing of polymer-graphite-based bipolar plates, their fabrication is usually limited to the compression of fine polymer-graphite powder mixtures. Graphite consists of large, two-dimensional (2D) honeycomb sheets stacked in the vertical direction that orient parallel to the plate surface under high-pressure compression. This alignment creates a material with greater in-plane than through-plane electrical and thermal conductivity [12,13]. However, the through-plane properties are more important for bipolar plates in fuel-cell stacks, because the electrical pathways run perpendicular to the plates. Several methods have been proposed to improve the through-plane properties. For example, more conductive carbon materials, such as carbon nanotubes, graphene, and carbon black, have been added as secondary fillers to establish an electrical pathway between graphite sheets [14-21]. However, the incorporation of secondary fillers requires extra processing, and the resulting improvements in the through-plane properties are not high enough for fuel-cell applications.

†To whom correspondence should be addressed.
E-mail: psy@knu.ac.kr

Another method of improving the through-plane properties is to change the orientation of graphite in the composite plate. Park and coworkers used a specially designed L-shaped extruder to prepare a high-performance polymer/vertically arranged graphite composite plate [8]. Laminar flow of the molten composite without turbulence was triggered by vertical compression of the stacked graphene nanoflakes, which were oriented perpendicular to the flow direction. The researchers noted significant improvements in through-plane thermal conductivity when the graphite was oriented in the vertical direction. However, the process required modification of the extruder and had limited potential for commercial application. In particular, Dweiri and Sahari prepared compression-molded polypropylene-graphite composite bipolar plates by using both melt compounding and solution blending methods [33,34]. The conductivity of the specimens prepared from the solution-blended mixtures was higher than that prepared by melt compounding because homogeneous mixing is difficult during melt compounding. The solution-blending method led to the formation of well-dispersed mixtures which result in good electrically conductive paths, but the disposal of organic solvents after the process presented a major disadvantage. However, they did not study the through-plane electrical conductivity, which may be reduced as compared to the in-plane electrical conductivity by parallel orientation of the graphite during solution sample preparation. The through-plane electrical conductivity of the melt-compounded sample may be improved because compounding can cause random orientation of the graphite in the polymer matrix due to the shearing force. Thus, studies on three-dimensional morphology combined with the through-plane and in-plane electrical conductivities are essential to understand the structure-property relationship. Table S2 shows a detailed comparison of the bipolar plate developed in this work with those reported in literature. PPS-graphite composites have good in-plane electrical conductivity and low density, which is advantageous for the reduction of the weight of the bipolar plate. Fluoroethylene propylene (FEP) is a crystalline fluoropolymer with excellent chemical resistance, but its flexural strength and electrical conductivity are lower than those of PPS. In addition, it has a high thermal coefficient of expansion and relatively low dimensional stability. Thermoset polymers such as epoxy and phenolic resins have excellent thermal and physical properties, but are susceptible to cracks in the fuel cell bipolar plate if used at high temperatures for a long time. Polypropylene (PP) is a common plastic that has poorer physical properties compared to the previously mentioned engineering plastics. The low melting point of PP (130 °C) makes it unsuitable for use in PAFC as the continuous operating temperature is 200 °C.

In this work, polymer-graphite composite samples were prepared with either a planar or relatively random graphite orientation from fine PPS-graphite powder mixtures by employing compression or extrusion-compression processing techniques, respectively. After confirming how the processing method affected the graphite orientation in the PPS-graphite plate, we explored in detail how the graphite orientation influenced the electrical, thermal, and mechanical properties. The anisotropy of properties in the compressed and extruded-compressed samples was investigated to determine the effect of shearing during extrusion on the anisotropic orientation. To further examine the extrusion process, the effect of PPS particle size on the performance of the bipolar plate was also explored. Studies on the anisotropic electrical conductivity of polymer-graphite composite samples are important for bipolar-plate applications. In particular, improvement of the through-plane electrical conductivity is essential for compressed samples. The shearing during compounding can cause random orientation of the graphite, resulting in the change of anisotropic properties to more isotropic ones. Studies on the orientation of the graphite in the composite are important for understanding the structure-property relationship. In this work, the three-dimensional structure of the graphite in the composite was studied using X-ray diffraction with different X-ray beams from different directions incident on the sample. The findings are expected to offer insight into the effect of conductive 2D filler orientation on the anisotropic properties of the resultant material. In addition, as no systematic studies have yet been performed on the structure-property relationship of PPS-graphite composites with high amounts of graphite, this study provides fundamental information on PPS-graphite composites that is missing from the literature.

EXPERIMENTAL

1. Materials

For the polymer-graphite composites, PPS powder (L2120, Toray, Japan) was selected as the matrix material. The thermal and electrical conductivity of pure PPS was 0.25 W m^{-1} k^{-1} and 1.5×10^{-16} S cm^{-1}, respectively. The raw PPS powder had large particles and a wide size distribution (40-2,000 μm); therefore, ground powder with an average particle size of approximately 20 μm was prepared by grinding the raw PPS powder in a porcelain bowl filled with liquid nitrogen for 40 min using a mortar and pestle.

Graphite powder with an average particle diameter of 500 μm (#3763, Asbury Carbons, USA) (see Supplementary Fig. S1) was used as purchased without further purification. The number of defects in the graphite powder was characterized by the ratio of intensities of the D and G bands (I_D/I_G ratio) located at 1,353 and 1,575 cm^{-1}, respectively, in the Raman spectrum. The I_D/I_G ratio of the graphite particles was 0.054 (see Supplementary Fig. S2), indicating that the graphite used in the study was relatively defect-free. Raman spectroscopy experiments were performed on the graphite and composite samples (ϕ=40 wt%) to study the structure of graphite in the composite. Fig. S3 shows the Raman spectra of PPS-graphite$_{com}$ and PPS-graphite$_{ext}$. The clear D and G peaks representing the defects in the graphitic structure and the E_{2g} phonon at the Brillouin zone center, respectively, are clearly observed. I_D/I_G ratios of the graphite and composite samples are 0.01 and 0.05, respectively, thus indicating that the graphitic structure remains virtually unchanged during the preparation of the composite.

2. Fabrication of PPS-graphite Composites by Melt Processes

Uniformly mixed PPS-graphite powders with different graphite concentrations (ϕ=10, 20, 30, and 40 wt%) were prepared by milling for 12 h with zirconia balls (diameter: 18 mm) using a ball mill (LM-BD4530, LK Lab, Korea). Then, PPS-graphite plate samples were prepared from these powders by either compression or extrusion-compression. The basic process and morphology control are

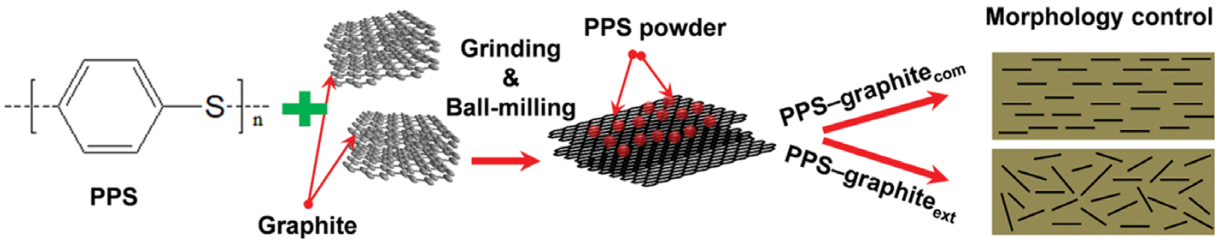

Fig. 1. Schematic of the preparation process of PPS-graphite$_{com}$ and PPS-graphite$_{ext}$ composites.

illustrated in Fig. 1.

For the compressed plate samples (hereafter referred to as PPS-graphite$_{com}$), ball-milled PPS-graphite powders with graphite concentrations of ϕ=10, 20, 30, and 40 wt% were directly compressed into samples. Compression was carried out at 300 °C under 2,000 psi for 1 h using a compression mold (HT-10T, ILSHIN Autoclave, Korea) consisting of a hollow cylindrical alloy mold (SKD-11C) (inner diameter: 6 cm; outer diameter: 7 cm; height: 2 cm) and a cylindrical rod (diameter: 6 cm; height: 3 cm). The cylindrical rod fitted tightly inside the mold. After compression, the samples were slowly cooled to 20 °C at a rate of −7 °C min^{-1}. To easily detach the samples from the mold, a polyimide film (thickness: 100 μm) was inserted between the sample and mold prior to compression.

For the extruded-compressed plate samples (hereafter referred to as PPS-graphite$_{ext}$), ball-milled PPS-graphite powders with graphite concentrations of ϕ=10, 20, 30, and 40 wt% were compounded using a twin-screw extruder (HAAKE^{TM} MiniLab 3 Micro Compounder, Thermo Fisher Scientific, USA) at 290 °C and a screw speed of 100 rpm for 10 min. The extruded material was then chopped into pellets, and subsequently compressed into samples following the compression process described above. The limited capacity of the mini-extruder restricted the graphite concentration to less than 40 wt%.

3. Characterization

The fracture surfaces and polished surfaces of the PPS-graphite composites were observed using field-emission scanning electron microscopy (FE-SEM; S-4800, Hitachi, Japan) and optical microscopy (BX51, Olympus, Japan), respectively. A four-probe tester (MST 4000A, MSTech, South Korea) and a source meter (2400, Keithley, USA) were used to measure the sheet resistance (R_s) distributions in PPS-graphite$_{com}$ (ϕ=40 wt%) disk specimens (diameter: 60 mm; thickness: 10 mm). In-plane and through-plane electrical conductivity measurements (RS8-10, Dasoleng, South Korea) were carried out on PPS-graphite$_{com}$ and PPS-graphite$_{ext}$ specimens (width: 5.6 mm; thickness: 4.8 mm; length: 12.7 mm); the specific resistance of each specimen was measured with an applied current of 100 mA from both ends and converted to conductivity. Based on the recommendations outlined in the international standard ASTM D790, the flexural strengths of PPS-graphite$_{com}$ and PPS-graphite$_{ext}$ bar specimens (width: 5 mm; length: 25 mm; thickness: 5 mm) were measured five times using a universal testing machine (UTM; ST-1001, SALT, South Korea) at a loading speed of 10 mm min^{-1} and loading force of 100 kgf. The particle-size distribution of the graphite and PPS powders was measured with different particle size analyzers (Mastersizer 2000, Malvern Panalytical, UK; and LS-13300, Beckman coulter, USA, respectively). The PPS measurements used a 25-mV helium-neon laser (632.8 nm) as the light source. Raman spectra of the PPS-graphite powders were obtained using a high-resolution Raman spectrometer (US/HR800, HORIBA Jobin Yvon, Japan) with an excitation wavelength of 532 nm. The thermal diffusivity was measured using a thermal conductivity meter (LFA457 Microflash, NETZSCH, Germany) on composite disk specimens (diameter: 18 mm; thickness: 5 mm) according to ASTM E1461. Thermogravimetric analyses (TGA; Q500, TA instruments, USA) of PPS, PPS-graphite$_{com}$, and PPS-graphite$_{ext}$ were performed over the temperature range of 25-900 °C in a nitrogen atmosphere at a scanning rate of 10 °C min^{-1}. Wide angle X-ray scattering (WAXS) patterns were obtained on the 9A beamline at the Pohang Light Source (PLS, South Korea) at a wavelength of 0.62 Å, a power of 11.04 keV, and a sample-to-detector distance of 220.5 mm. A 2D charge-coupled device (CCD) camera (Rayonix, USA) was used to collect the 2D WAXS patterns. One-dimensional (1D) patterns were obtained by scanning the 2D patterns with FIT-2D software (ERSF, France). The apparent crystal size was calculated using the Scherrer equation (Eq. (1)) along the (002)$_{graphite}$ direction of the PPS-graphite plate samples when the X-ray beam was parallel to the plate surface:

$$\text{Apparent crystal size} = \frac{0.9\times\lambda}{\beta\times\cos\theta}, \quad (1)$$

where λ, θ, and β are the wavelength of the radiation, the Bragg angle, and full width at half maximum (FWHM) of the peak, respectively.

RESULTS AND DISCUSSION

1. Preparation of PPS-graphite Powders

Figs. 2(a) and 2(b) show the particle-size distribution of the PPS powder before and after grinding, respectively. Fig. S4 shows the SEM images of these particles at low magnification. The PPS particles were large and had a wide size distribution (40-2,000 μm) before grinding (Fig. 2(a), Fig. S4(a)); after grinding, the average particle size was approximately 20 μm (Fig. 2(b), Fig. S4(b)). Grinding greatly affected the mixed PPS-graphite powder morphology after ball milling for 12 h. The raw PPS particles were of a comparable size to the graphite particles, which meant that their mixture consisted of large PPS particles interspersed between the graphite particles, as shown in the inset of Fig. 2(a). In contrast, the ground PPS particles were small enough to coat the graphite surface, as

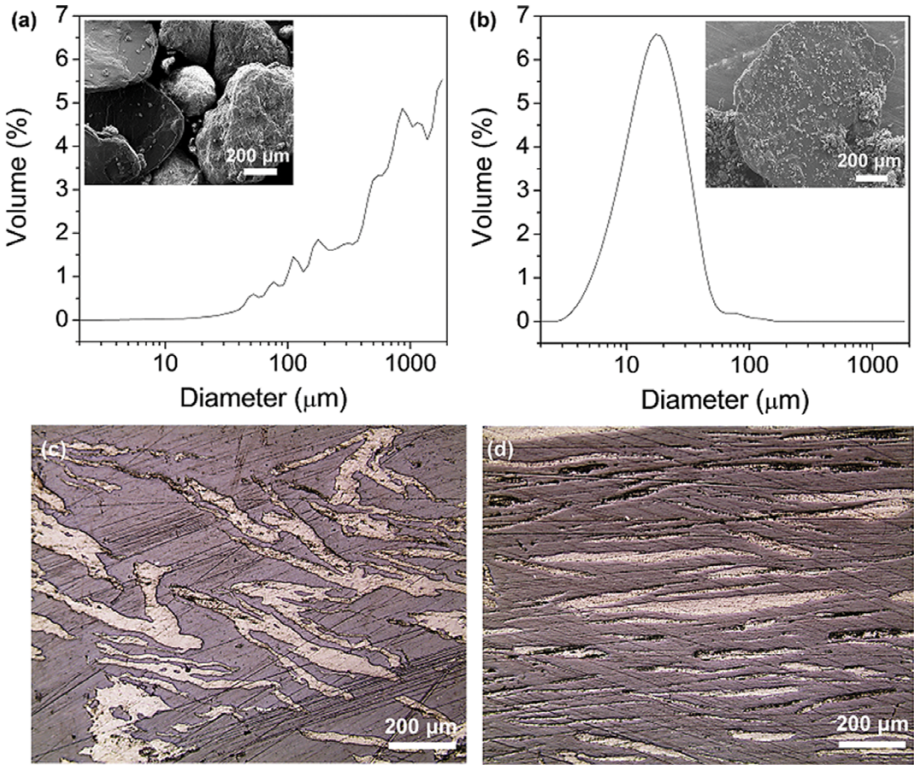

Fig. 2. (a), (b) Particle-size distributions of (a) raw and (b) ground PPS particles; the insets in (a), (b) are SEM images of the PPS-graphite mixture with graphite concentration of ϕ=40 wt% after ball milling for 12 h. (c), (d) Optical-microscope reflection-mode images of the polished surfaces of PPS-graphite$_{com}$ (ϕ=40 wt%) when (c) raw and (d) ground PPS particles were used; the pressure was applied in the vertical direction during sample preparation. The white and black parts represent graphite and PPS, respectively.

shown in the inset of Fig. 2(b). It is likely that the small PPS particles coat the graphite in this way owing to interfacial interactions between the large graphite sheets and small polymer particles during high-energy ball milling. Figs. 2(c) and 2(d) show optical-microscope reflection-mode images of polished surfaces of PPS-graphite$_{com}$ (ϕ=40 wt%) when raw and ground PPS particles were used, respectively. The white and black parts indicate the graphite and PPS, respectively. The sample prepared with raw PPS particles consisted of irregular graphite particles that were not well-dispersed in the PPS matrix, while in the sample prepared with ground PPS particles, the graphite had a parallel orientation and good dispersion. Thus, grinding the PPS powder is necessary to obtain uniformly distributed and oriented graphite sheets in the PPS matrix for bipolar-plate application. The elemental analysis results obtained using XPS full-scan spectra are presented in Fig S5. Table S1 lists the C1s peak parameters with the corresponding binding energies. For pristine graphite, the C(1), C(2), C(3), and C(4) peaks were observed at 284.5, 285.4, 286.4, and 287.4 eV, respectively, which correspond to sp^2 carbons, sp^3 carbons, sp^3 carboxyl groups, and C=O, respectively. Most carbon atoms are in the sp^2 state (87.5%), indicating that pristine graphite is mostly composed of the graphitic π conjugated structure. A small amount of sp^3 carbons (7.3%) are present at the edge of the graphite. The presence of the O-C (carboxyl) and C=O peaks is because of the small amount of oxygen which is usually observed in used natural graphite.

The effects of particle size on the electrical conductivity, mechanical strength, and inertness to phosphoric acid, which are important properties for bipolar plates in phosphoric acid fuel cells, were studied. Figs. 3(a(i)) and 3(a(ii)) show the sheet resistance distributions of PPS-graphite$_{com}$ (ϕ=40 wt%) prepared with raw and ground PPS particles, respectively, at points with 0.8 mm separation in a 5×5 matrix. The sheet resistance of PPS-graphite$_{com}$ prepared with raw PPS particles varied from one position to another (Fig. 3(a(i))), while that of the sample prepared with ground PPS particles was quite uniform throughout the matrix (Fig. 3(a(ii))). This demonstrates that large PPS particles should be ground to a small size before use when fabricating bipolar plates.

The flexural strengths were quite similar for the samples prepared from raw and ground PPS particles (Fig. 3(b)), possibly because PPS already has good mechanical properties, so the dispersion of graphite did not significantly affect the mechanical properties of the resulting composite. The inertness of the samples to phosphoric acid was tested by measuring the weight gain (Δg) after immersion in phosphoric acid (85%) at 150 °C for 24 h (Fig. 3(c)). The weight gain can be attributed to the phosphoric acid that has infiltrated the sample. The weight gain of the PPS-graphite$_{com}$ sample prepared from raw PPS particles was Δg=1.51 wt%, while that of the sample prepared from ground PPS particles was Δg=0.85 wt%, indicating that grinding the PPS particles imparted good chemical inertness to the composite. This may be because there was more space at the graphite-matrix interface when raw PPS particles were used, which facilitated the infiltration of phos-

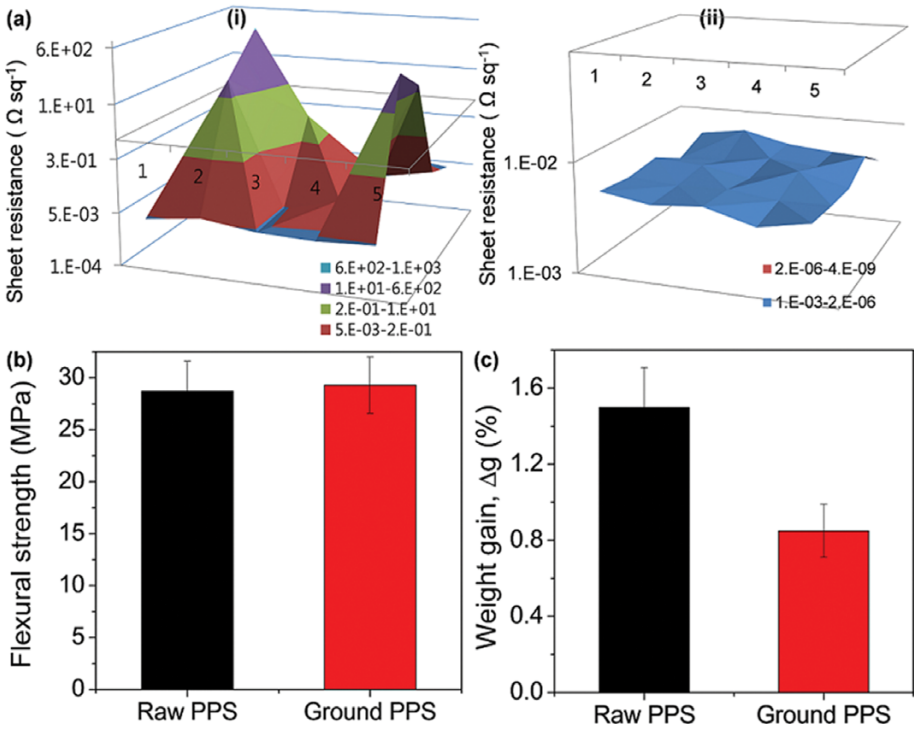

Fig. 3. (a) Electrical conductivity at points with 0.8 mm separation in a 5×5 matrix, (b) flexural strength, and (c) weight gain (Δg) in phosphoric acid of PPS-graphite$_{com}$ (ϕ=40 wt%) prepared with (i) raw and (ii) ground PPS particles. The weight gain is defined as $\Delta g=(g-g_0)/g_0\times100$, where g is the weight after immersing PPS-graphite$_{com}$ in phosphoric acid (85%) at 150 °C for 24 h, and g_0 is the initial weight.

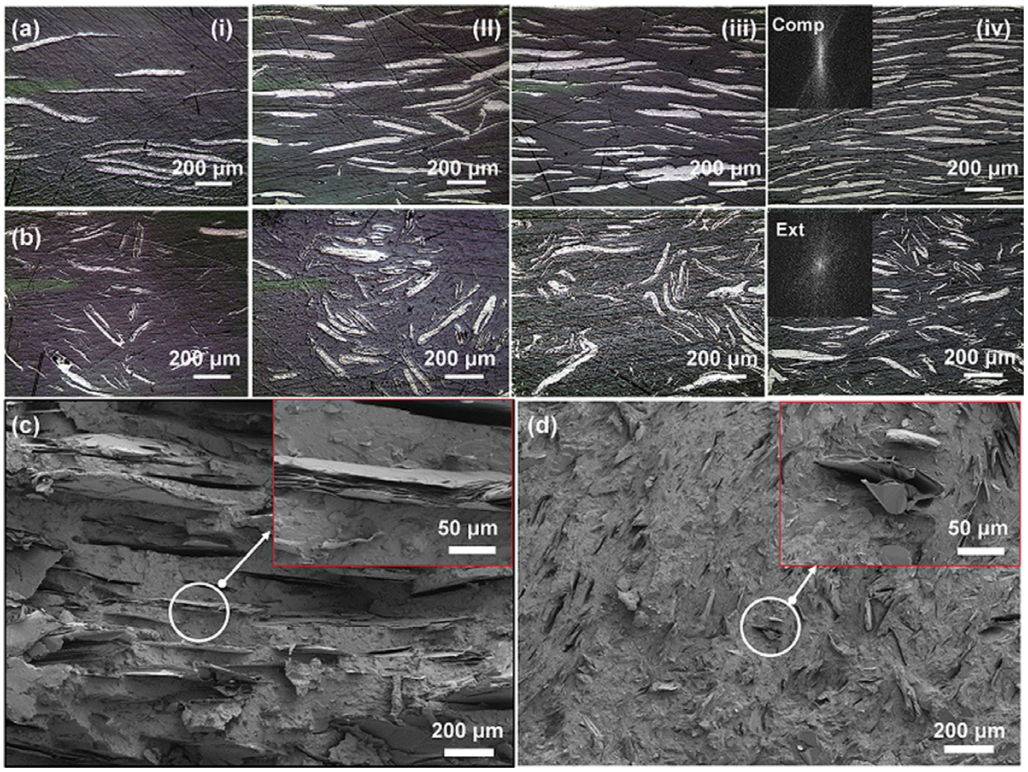

Fig. 4. (a), (b) Optical-microscope reflective-mode images of the polished surfaces of (a) PPS-graphite$_{com}$ and (b) PPS-graphite$_{ext}$ with a graphite composition (ϕ) of (i) 10, (ii) 20, (iii) 30, and (iv) 40 wt%. The pressure was applied in the vertical direction during sample preparation. The insets in (iv) show the Fourier transform images. (c), (d) SEM images of fractured surfaces of (c) PPS-graphite$_{com}$ and (d) PPS-graphite$_{ext}$ (both at ϕ=40 wt%); the insets show magnified views of the circled regions.

phoric acid.

2. Morphology of PPS-graphite$_{com}$ and PPS-graphite$_{ext}$ Composites

Fig. 4(a) shows optical-microscope reflective-mode images of polished surfaces of the PPS-graphite$_{com}$ samples (ϕ=10, 20, 30, and 40 wt%). Pressure was applied to the sample in the vertical direction during compression, causing the graphite sheets to orient parallel to the plate surface. The inset of Fig. 4(a(iv)) shows a Fourier transform image of the sample with ϕ=40 wt%. The scattering along the vertical direction indicates that the graphite sheets were oriented parallel to the sample surface. The anisotropic orientation of the graphite sheet was observed even when ϕ=10 wt% because the large graphite sheets effectively transfer the compressive forces, orienting them parallel to the plate surface. These anisotropic orientations may have caused the anisotropic properties observed in the PPS-graphite$_{com}$ sample.

The PPS-graphite powder was compounded by an extruder prior to compression to produce PPS-graphite$_{ext}$ composite plate samples with a random graphite orientation. Fig. 4(b) shows optical-microscope reflective-mode images of the ground and polished surfaces of the PPS-graphite$_{ext}$ samples with ϕ of 10, 20, 30, and 40 wt%; it can be seen that the graphite sheets were relatively randomly oriented. The Fourier transform image of the sample with ϕ=40 wt% also shows more random scattering of the graphite sheets, indicating that the shear force during compounding caused the graphite to orient randomly. This random orientation is likely to alter the properties of the PPS-graphite$_{ext}$ sample in comparison to the PPS-graphite$_{com}$ sample. Notably, at ϕ=40 wt%, many of the graphite sheets were clearly bent, suggesting that bending deformation of the sheets occurred during compounding.

The morphology of the composites was studied in more detail via SEM after fracturing the samples. Fig. 4(c) shows an SEM image of the PPS-graphite$_{com}$ fracture surface (ϕ=40 wt%). The image clearly shows the large, parallel oriented graphite sheets, with an undeformed layered graphitic structure. Fig. 4(d) shows an SEM image of the PPS-graphite$_{ext}$ fracture surface (ϕ=40 wt%). Randomly oriented graphite sheets can be seen, with clear deformation related to the bent structure seen in the optical-microscope reflective-mode image in Fig. 4(b). This deformed graphite structure may deteriorate the electrical properties of the composite.

To analyze the graphite orientation on an atomic scale, WAXS patterns were obtained when the X-ray beams were parallel and perpendicular to the surface of the PPS-graphite plate samples. Fig. 5(a) shows typical examples of WAXS patterns of PPS-graph-

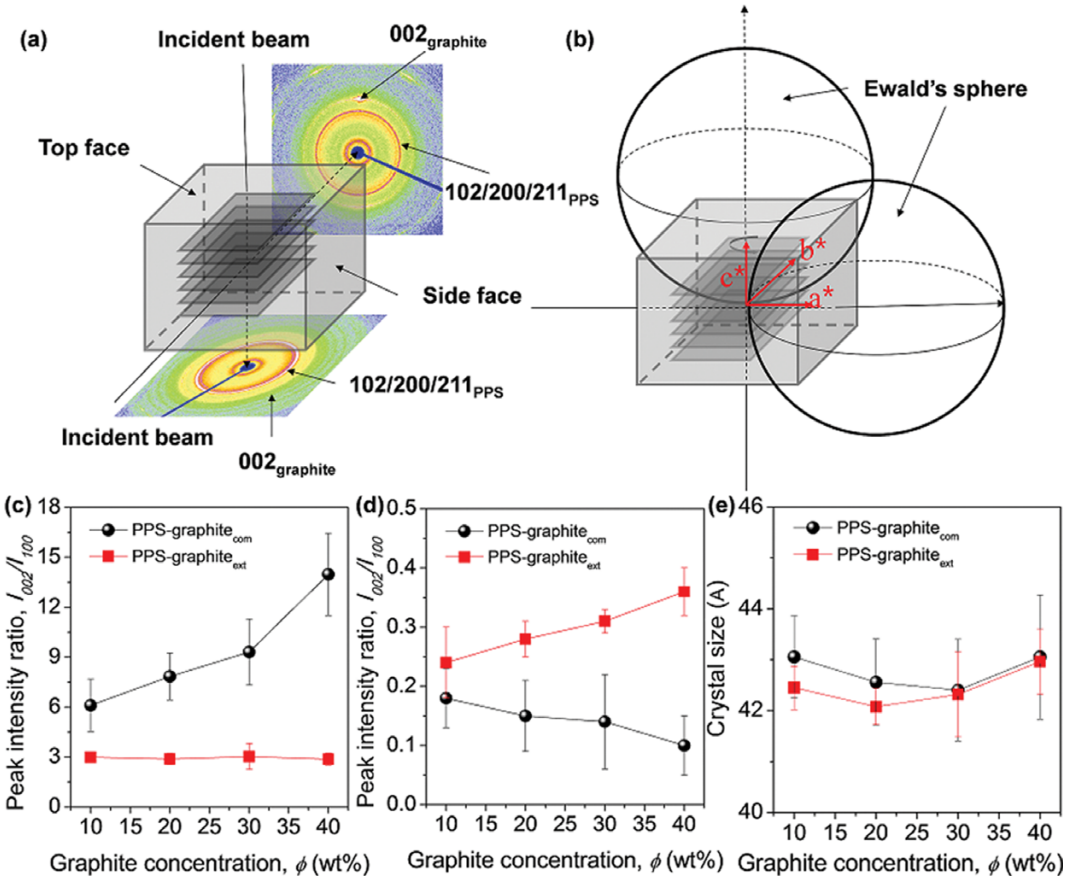

Fig. 5. Schematic of (a) the collection of WAXS patterns and (b) Ewald spheres of the PPS-graphite composite when the X-ray beam is parallel and perpendicular to the sample surface. (c), (d) Values of I_{002}/I_{100} of PPS-graphite$_{com}$ (closed circles) and PPS-graphite$_{ext}$ (open circles) (both at ϕ=40 wt%) when the X-ray beam was (c) parallel and (d) perpendicular to the sample surface. (e) Apparent crystal size along the (002)$_{graphite}$ direction of PPS-graphite$_{com}$ (closed circles) and PPS-graphite$_{ext}$ (open circles) (both at ϕ=40 wt%) when the X-ray beam was parallel to the sample surface.

ite$_{com}$ (ϕ=40 wt%), which had graphite sheets oriented parallel to the sample surface. Two sets of reflections from PPS and graphite were observed. The 102/200/211 reflections of PPS at 2θ=20.48° were circular when the X-ray beam was both parallel and perpendicular to the film surface, indicating that the PPS crystals were oriented almost randomly—the relaxation of PPS is too fast to maintain the planar orientation of the PPS chains obtained by compressive force [27]. However, the 002 reflection of graphite at 2θ=26.65° was oriented along the normal direction of the sample surface when the X-ray beam was parallel to the sample surface, indicating that the graphite layers were oriented parallel to the sample surface. This 002 reflection of graphite was nearly undetectable when the X-ray beam was perpendicular to the sample surface.

The origin of the difference in the 002 reflection of PPS-graphite$_{com}$ according to X-ray beam direction can be explained by Ewald spheres. Fig. 5(b) shows the Ewald spheres when the X-ray beams are parallel and perpendicular to the sample surface. The graphite layers are oriented parallel to the sample surface. The c* direction of the graphite represents the 002 direction of the reciprocal lattice. When the reciprocal lattice point is in contact with the Ewald sphere, a reflection can be recorded. However, when the X-ray beam is perpendicular to the sample surface, the reciprocal lattice point of the 002 reflection is inside the Ewald sphere. Hence, it is difficult to be touched by the Ewald sphere, i.e., it is difficult to be reflected. In contrast, when the X-ray beam is parallel to the sample surface, the reciprocal lattice point of the 002 reflection is close to the Ewald sphere. It can therefore be more easily touched by the Ewald sphere and hence reflected. The basal planes of the graphite crystal (hk0 reflections) are close to the Ewald sphere even when the X-ray beam is perpendicular to the sample surface. The basal 100 reflection of graphite in PPS-graphite$_{com}$ was observed when the X-ray beam was both perpendicular and parallel to the sample surface; therefore, the 100 reflection could be used for normalization of the 002 reflection. Thus, the ratio between the intensities of the 002 and 100 reflections (I_{002}/I_{100}) of graphite represents the degree of planar orientation of the graphite layers in the sample.

Figs. 5(c) and 5(d) show the I_{002}/I_{100} ratios of PPS-graphite$_{com}$ and PPS-graphite$_{ext}$ (ϕ=40 wt%) when the X-ray beam was parallel and perpendicular to the sample surface, respectively. With the parallel X-ray beam (Fig. 5(c)), the I_{002}/I_{100} value for PPS-graphite$_{com}$ was much higher than that for PPS-graphite$_{ext}$ (13.98 vs. 2.47). Conversely, it was much lower (0.1 vs. 0.36) with the perpendicular X-ray beam (Fig. 5(d)). These results indicate that the planar orientation was well-defined in PPS-graphite$_{com}$ compared to that in PPS-graphite$_{ext}$, as predicted by the morphological studies. Thus, the I_{002}/I_{100} ratio of a PPS-graphite composite could be used to determine its degree of planar orientation by utilizing X-ray beams that are either parallel or perpendicular to the sample surface. However, the perpendicular I_{002}/I_{100} ratio is notably small when the degree of planar orientation is considerably high, as shown in the

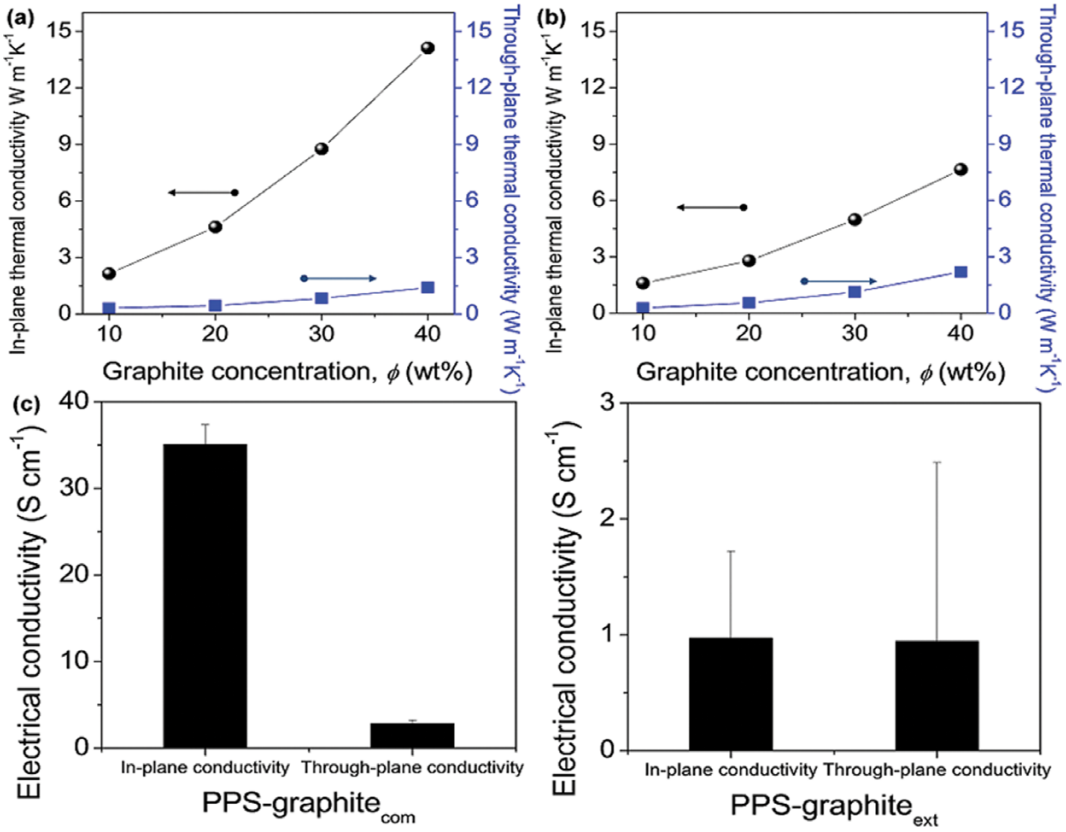

Fig. 6. (a), (b) In-plane and through-plane thermal conductivities of (a) PPS-graphite$_{com}$ and (b) PPS-graphite$_{ext}$ as functions of ϕ. (c) In-plane and through-plane electrical conductivities of PPS-graphite$_{com}$ and PPS-graphite$_{ext}$ (both at ϕ=40 wt%); the inset shows a magnified view of the data of PPS-graphite$_{ext}$.

discussion of the Ewald sphere. For example, the I_{002}/I_{100} ratio of the PPS-graphite$_{com}$ sample (ϕ=40 wt%) was only 0.1 when the X-ray beam was perpendicular to the plate surface. Hence, the parallel I_{002}/I_{100} ratio of the PPS-graphite$_{com}$ sample was more accurate. Thus, the planar orientation could be more accurately determined by utilizing a parallel X-ray beam.

The planar orientation of PPS-graphite$_{com}$ continuously increased as ϕ increased, as shown in Fig. 5(c), because the pressure during compression was more effectively transferred to the graphite sheets when ϕ was high. However, the planar orientation of PPS-graphite$_{ext}$ was low and nearly constant regardless of ϕ, because the graphite was already randomly oriented in the PPS matrix by extrusion prior to compression to form the plate sample. Thus, a more isotropic structure could be obtained from extrusion-compression than from compression alone. The apparent crystal size was calculated using the Scherrer equation (Eq. (1)) along the $(002)_{graphite}$ direction of PPS-graphite$_{com}$ and PPS-graphite$_{ext}$ samples (ϕ=40 wt%) with a parallel X-ray beam (Fig. 5(d)). The apparent crystal size of PPS-graphite$_{com}$ was slightly larger than that of PPS-graphite$_{ext}$, indicating that the shearing force during compounding was enough to peel off the graphite layers. This occurred owing to the small capacity of the extruder, which limits the amount of filler that can be incorporated (in this case to about 40 wt% graphite).

3. Physical Properties of PPS-graphite$_{com}$ and PPS-graphite$_{ext}$ Composites

The thermal conductivity of a polymer-graphite composite is strongly correlated with the orientation of graphite in the polymer matrix [28-32]. Fig. 6(a) shows the in-plane and through-plane thermal conductivities of PPS-graphite$_{com}$ (with a parallel graphite orientation) as a function of ϕ. The in-plane thermal conductivity was significantly higher than the through-plane thermal conductivity. For example, at ϕ=40 wt%, the in-plane thermal conductivity was 14.12 W m^{-1} K^{-1}, while the through-plane conductivity was only 1.41 W m^{-1} K^{-1}. This high anisotropic thermal conductivity was due to the high planar orientation in the PPS-graphite$_{com}$ composite. The difference between the in-plane and through-plane thermal conductivities increased with increasing ϕ, along with the increasing degree of planar orientation (see Fig. 5).

Fig. 6(b) shows the in-plane and through-plane thermal conductivities of PPS-graphite$_{ext}$ as a function of ϕ. The random orientation provided isotropy, causing the in-plane thermal conductivity to be only slightly higher than the through-plane conductivity. For example, at ϕ=40 wt%, the in-plane thermal conductivity was 7.65 W m^{-1} K^{-1}, whereas the through-plane thermal conductivity was 2.21 W m^{-1} K^{-1}. The difference between the in-plane and through-plane thermal conductivities was almost constant regardless of ϕ, because they were affected only by the amount of graphite; the effect of graphite orientation was negligible.

The electrical conductivity of the PPS-graphite composites was examined with regard to the graphite structure. Fig. 6(c) shows the in-plane and through-plane electrical conductivities of PPS-graphite$_{com}$ and PPS-graphite$_{ext}$ (ϕ=40 wt%). The electrical conductivity of PPS-graphite$_{com}$ was higher than that of PPS-graphite$_{ext}$ in both the in-plane and through-plane directions (35.08 and 2.82 vs. 0.97 and 0.94 S cm^{-1}, respectively). The higher conductivity of PPS-graphite$_{com}$ may be related to the destruction of the graphitic structure in PPS-graphite$_{ext}$ during compounding, as demonstrated in the SEM image in Fig. 4(d). However, for PPS-graphite$_{com}$, with a parallel orientation, the in-plane electrical conductivity was almost ten-times higher than the through-plane electrical conductivity. In contrast, there was not much difference between these values for the randomly oriented PPS-graphite$_{ext}$. Hence, the graphite orientation greatly affected the anisotropy of the electrical conductivity. Notably, the electrical conductivity was found to be more sensitive than the thermal conductivity to the graphite orientation.

The mechanical strength and thermal stability of PPS-graphite$_{com}$ and PPS-graphite$_{ext}$ were studied by examining the flexural strength and by conducting TGA, respectively. Fig. 7(a) shows the flexural strength of PPS-graphite$_{com}$ and PPS-graphite$_{ext}$ as a function of ϕ. The flexural strength of PPS-graphite$_{ext}$ was higher than that of PPS-graphite$_{com}$, with the difference between them increasing as ϕ increased. The planar orientation of graphite in the polymer matrix introduced weak points into the structure, which reduced the flexural strength of PPS-graphite$_{com}$ compared to that of PPS-graphite$_{ext}$. Fig. 7(b) shows TGA thermograms of PPS (ϕ=0 wt%), PPS-graphite$_{com}$ and PPS-graphite$_{ext}$ (both at ϕ=40 wt%). The thermal-degradation temperature (T_{deg}) was determined as the peak temperature of the differential curve of the TGA thermogram. The val-

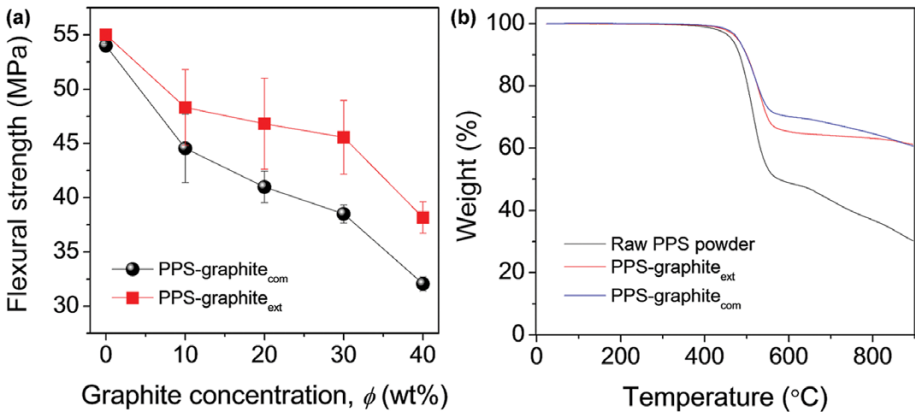

Fig. 7. (a) Flexural strength of PPS-graphite$_{com}$ and PPS-graphite$_{ext}$ as a function of ϕ. (b) TGA thermograms of PPS (ϕ=0 wt%), PPS-graphite$_{com}$, and PPS-graphite$_{ext}$ (both at ϕ=40 wt%).

ues of T_{deg} for PPS, PPS-graphite$_{com}$, and PPS-graphite$_{ext}$ were 515.7, 527.4, and 530.1 °C, respectively. The values of T_{deg} for PPS-graphite$_{com}$ and PPS-graphite$_{ext}$ were similar to each other, but they were both higher than that of pure PPS, indicating that the thermal stability was improved by adding graphite regardless of its orientation in the composite.

CONCLUSIONS

PPS-graphite$_{com}$ and PPS-graphite$_{ext}$ composite samples were prepared by compression and extrusion-compression, respectively, using ground PPS particles and graphite sheets. The composite samples were compared to investigate the effect of graphite morphology on the electrical and thermal conductivities. Grinding the large raw PPS particles to smaller particles with an average diameter of 18 μm imparted better inertness to phosphoric acid and more uniform electrical conductivity to the plate sample. The PPS-graphite$_{com}$ plate sample had highly anisotropic electrical and thermal conductivity because of the planar orientation of graphite in the PPS matrix, while the PPS-graphite$_{ext}$ plate sample exhibited more isotropic electrical and thermal conductivity. Thus, the through-plane conductivity of PPS-graphite$_{ext}$ was improved and closer to the in-plane properties. However, because of the defects generated by high shearing forces during extrusion, the in-plane conductivity of PPS-graphite$_{ext}$ was reduced compared to that of PPS-graphite$_{com}$. This reduction in in-plane property was greater for the electrical conductivity, because the electron pathway is more sensitive than the heat conducting pathway to the conducting honeycomb structure of graphite. The thermal stability of both PPS-graphite$_{com}$ and PPS-graphite$_{ext}$ was slightly improved compared to that of pure PPS, and the flexural strength of PPS-graphite$_{ext}$ was higher than that of PPS-graphite$_{com}$. This fundamental information on the relationship between the structure and properties of PPS-graphite composites is expected to aid in the design and fabrication of bipolar plates using a high-capacity extruder for fuel-cell applications.

ACKNOWLEDGEMENTS

This work was supported by the National Research Foundation of Korea (grant number NRF-2016M1A2A2937163) and the Korea Institute of Energy Technology Evaluation and Planning of Korea (grant number KETEP-20163010032040).

CONFLICT OF INTEREST

The authors declare that they have no conflict of interest.

NOMENCLATURE

I_D/I_G : ratio of intensities of the D and G bands
I_{002}/I_{100} : ratio of intensities of the 100 and 002 reflections of graphite
R_s : sheet resistance
ϕ : graphite concentration [wt%]
λ : wavelength of radiation
θ : Bragg angle
β : full width at half maximum (FWHM)
Δg : weight gain of the composite sample [wt%]

SUPPORTING INFORMATION

Additional information as noted in the text. This information is available via the Internet at http://www.springer.com/chemistry/journal/11814.

REFERENCES

1. S. H. Lee, N. Kakati, J. Maiti, S. H. Jee, D. J. Kalita and Y. S. Yoon, *Thin Solid Films*, **529**, 374 (2013).
2. H. Sun, K. Cooke, G. Eitzinger, P. Hamilton and B. Pollet, *Thin Solid Films*, **528**, 199 (2013).
3. B. D. Cunningham and D. G. Baird, *J. Power Sources*, **168**, 418 (2007).
4. S. Dhakate, R. Mathur, B. Kakati and T. Dhami, *Int. J. Hydrogen Energy*, **32**, 4537 (2007).
5. R. K. Pachauri and Y. K. Chauhan, *Int. J. Elec. Power*, **74**, 49 (2016).
6. C. Gao, S. Zhang, Y. Lin, F. Li, S. Guan and Z. Jiang, *Compos. Part B-Eng.*, **79**, 124 (2015).
7. H. Ma, B. Chu and B. S. Hsiao, *Eur. Polym. J.*, **87**, 398 (2017).
8. H. Jung, S. Yu, N. S. Bae, S. M. Cho, R. H. Kim, S. H. Cho, I. Hwang, B. Jeong, J. S. Ryu, J. Hwang, S. M. Hong, C. M. Koo and C. Park, *ACS Appl. Mater. Interfaces*, **7**, 15256 (2015).
9. M. H. Lee, H. Y. Kim, S. M. Oh, B. C. Kim, D. Bang, J. T. Han and J. S. Woo, *Int. J. Hydrogen Energy*, **43**, 21918 (2018).
10. N. H. Kim, T. Kuila, K. M. Kim, S. H. Nahm and J. H. Lee, *Polym. Test*, **31**, 537 (2012).
11. M. Park, J. H. Park, B. J. Yang, J. Cho, S. Y. Kim and I. Jung, *Compos. Part A Appl. Sci. Manuf.*, **109**, 124 (2018).
12. M. Khandelwal and M. M. Mench, *J. Power Sources*, **161**, 1106 (2006).
13. H. Suherman, A. B. Sulong and J. Sahari, *Ceram. Int.*, **39**, 1277 (2013).
14. H. Choi, J. S. Woo, J. T. Han and S.-Y. Park, *Nanotechnology*, **28**, 465706 (2017).
15. P. M. Ajayan, O. Stephan, C. Colliex and D. Trauth, *Science*, **265**, 1212 (1994).
16. U. Gubler, M. Raunhardt and A. Stump, *Thin Solid Films*, **515**, 1737 (2006).
17. W. Bauhofer and J. Z. Kovacs, *Compos. Sci. Technol.*, **69**, 1486 (2009).
18. N. Gamze Karsli, S. Yesil and A. Aytac, *Compos. Part B-Eng.*, **63**, 154 (2014).
19. M. Russello, E. K. Diamanti, G. Catalanotti, F. Ohlsson, S. C. Hawkins and B. G. Falzon, *Compos. Struct.*, **206**, 272 (2018).
20. M. Y. Zakaria, A. B. Sulong, J. Sahari and H. Suherman, *Compos. Part B-Eng.*, **83**, 75 (2015).
21. R. Zhang, A. Dowden, H. Deng, M. Baxendale and T. Peijs, *Compos. Sci. Technol.*, **69**, 1499 (2009).
22. R. Ghasemi and L. Elmquist, *Wear*, **320**, 120 (2014).
23. P. Pötschke, T. D. Fornes and D. R. Paul, *Polymer*, **43**, 3247 (2002).
24. E. T. Thostenson and T. W. Chou, *J. Phys. D: Appl. Phys.*, **35**, L77 (2002).
25. T. Derieth, G. Bandlamudi, P. Beckhaus, C. Kreuz, F. Mahlendorf and A. Heinzel, *J. New Mater. Electrochem. Syst.*, **11**, 21 (2008).

26. R. B. Mathur, S. R. Dhakate, D. K. Gupta, T. L. Dhami and R. K. Aggarwal, *J. Mater. Process. Technol.*, **203**, 184 (2008).
27. J. Guo, Y. Liu, R. Prada-Silvy, Y. Tan, S. Azad, B. Krause, P. Pötschke and B. P. Grady, *J. Polym. Sci. B Polym. Phys.*, **52**, 73 (2014).
28. J. Xing, Q.-Q. Ni, B. Deng and Q. Liu, *Compos. Sci. Technol.*, **134**, 184 (2016).
29. A. Ameli, P. U. Jung and C. B. Park, *Compos. Sci. Technol.*, **76**, 37 (2013).
30. Y. Jia, H. He, Y. Geng, B. Huang and X. Peng, *Compos. Sci. Technol.*, **145**, 55 (2017).
31. M. Karimi, R. Ghajar and A. Montazeri, *Compos. Struct.*, **201**, 528 (2018).
32. P. Ding, J. Zhang, N. Song, S. Tang, Y. Liu and L. Shi, *Compos. Sci. Technol.*, **109**, 25 (2015).
33. R. A. Antunes, M. C. L. De Oliveira, G. Ett and V. Ett, *J. Power Sources*, **196**, 2945 (2011).
34. F. G. B. San and G. Tekin, *Int. J. Energy Res.*, **37**, 283 (2013).
35. M. Xiao, Y. Lu, S. J. Wang, Y. F. Zhao and Y. Z. Meng, *J. Power Sources*, **160**, 165 (2006).
36. H. S. Lee, H. J. Kim, S. G. Kim and S. H. Ahn, *J. Mater. Process. Technol.*, **187**, 425 (2007).
37. R. Dweiri and J. Sahari, *J. Power Sources*, **171**, 424 (2007).

Supporting Information

Poly(phenylene sulfide)-graphite composites for bipolar plates with preferred morphological orientation

Ho-Joon Park*, Jong Seok Woo, and Soo-Young Park*,†**

*Department of Polymer Science & Engineering, Polymeric Nanomaterials Laboratory, School of Applied Chemical Engineering, Kyungpook National University, 80 Daehak-ro, Buk-gu, Daegu 41566, Korea
**Advanced Center of Engineering, Morgan Advanced Materials, 23, Dalseong2cha 4-ro, Guji-myeon, Dalseong-gun, Daegu 43013, Korea
(*Received 25 July 2019 • accepted 26 September 2019*)

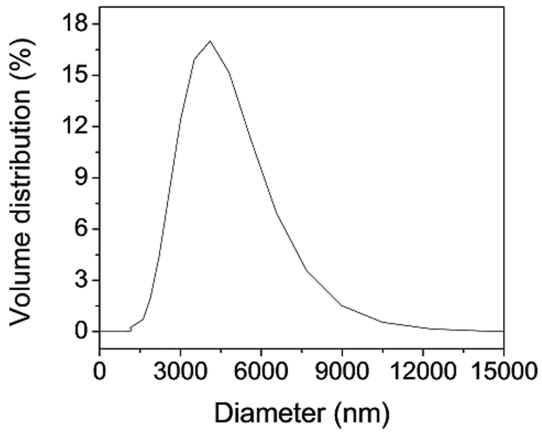

Fig. S1. Particle size distribution of graphite used in this study.

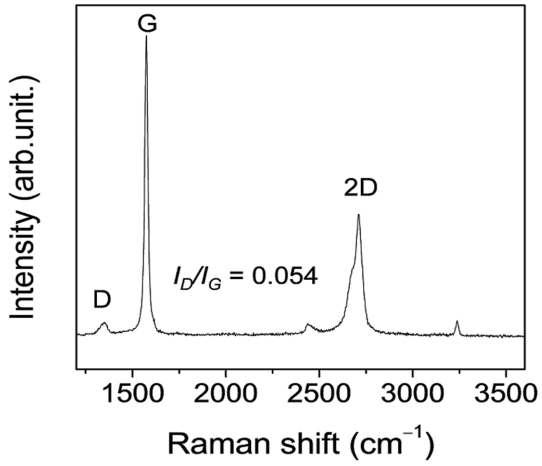

Fig. S2. Raman spectrum of graphite used in this study.

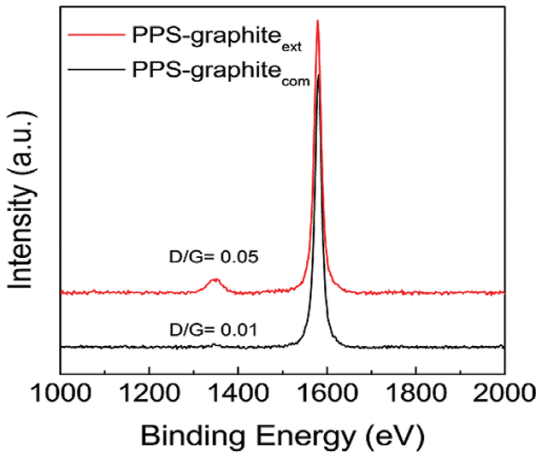

Fig. S3. Raman spectra of PPS-graphite$_{com}$ and PPS-graphite$_{ext}$ (both at ϕ=40 wt%).

Table S1. C1s peak parameters of pristine graphite

	Component	Peak position (eV)	Concentration (%)
C(1)	C-C (sp^2)	284.5	87.5
C(2)	C-C (sp^3)	285.5	7.3
C(3)	O-C (carboxyl)	286.4	2.4
C(4)	C=O	287.4	2.9

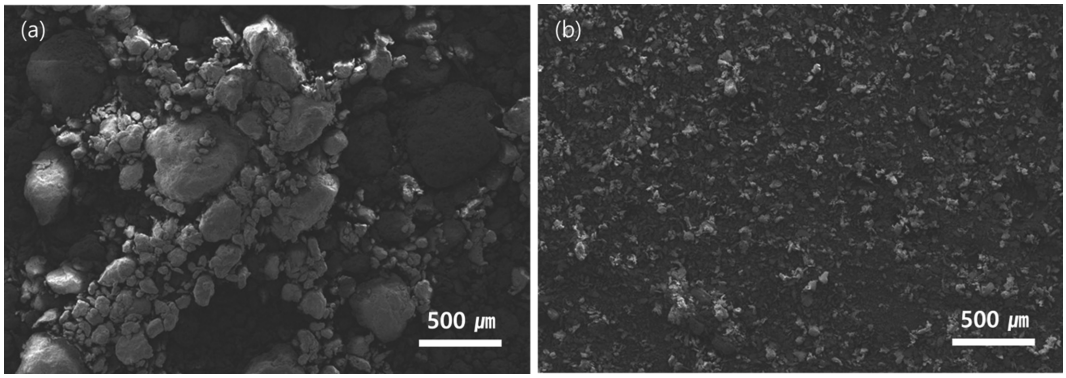

Fig. S4. SEM images of the (a) raw and (b) ground PPS particles at low magnification.

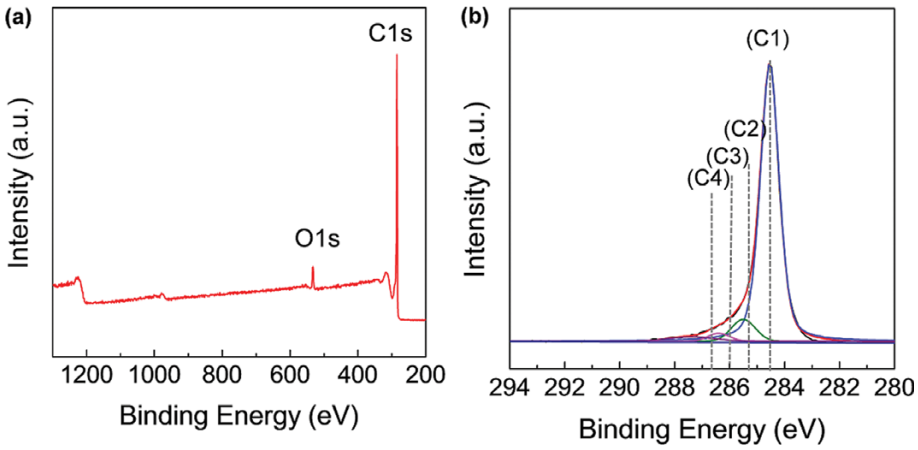

Fig. S5. (a) XPS full-scan spectrum of pristine graphite and (b) deconvoluted C1s core-level XPS spectra of (a).

Table S2. Comparison of the composite bipolar plate developed in this study with those reported in related literature

Polymer	Filler		Filler orientation	Thermal conductivity (W m^{-1} K^{-1})		Electrical conductivity (S cm^{-1})		Flexural strength (MPa)	Ref.
	Type	Content (wt%)		Through-plane	In-plane	Through-plane	In-plane		
PPS	NG[e]	40	Random (Extruded)	2.2	7.7	0.8	0.9	38	This work
			Parallel	1.4	14.1	3	35	32	This work
PPS	NG[e]	40	Parallel	-	-	-	0.1	18	10
PPS	SG[f]	40	Partially random	-	-	-	1	23	10
	CB[a]	3							
PVDF[b]	GNF[c]	40	Random	1.8	-	-	-	-	8
			Perpendicular	10.1	-	-	0.4	-	8
FEP[d]	NG[e]	40	Perpendicular	-	-	-	0.2	12	9
Epoxy	SG[f]		Parallel	-	-	-	35	4	35
Phenolic	NG[e]	65	Parallel	-	-	-	-	38	36
PP	CB[a], NG[e]	80	Parallel	-	-	-	35	-	37

-, Not available
[a]Carbon black
[b]Poly(vinylidene fluoride)
[c]Graphene nano-flake
[d]Fluorinated ethylene propylene
[e]Natural graphite
[f]Synthetic graphite